Low-Speed Control for Permanent-Magnet DC Torque Motor Using Observer-Based Nonlinear Triple-Step Controller

Hongqing Chu, Bingzhao Gao, Wanli Gu, and Hong Chen, *Senior Member, IEEE*

***Abstract*—In speed control of a permanent-magnet dc torque motor, cogging torque is an undesirable disturbance and results in speed ripple. It is especially prominent at lower speeds, with the symptom of jerkiness. This paper provides a novel observer-based nonlinear triple-step controller to improve the low-speed tracking performance. Considering that cogging torque is a fast time-varying disturbance and changes harmonically, a nonlinear parameter-varying high-order system is established to model the fast-varying properties of cogging torque. Then, a reduced-order nonlinear observer is designed to estimate the cogging torque, and the robustness analysis with regard to the uncertainties is given for the proposed nonlinear observer. Thereafter, a triple-step nonlinear method is applied to derive a speed tracking controller, and then the robustness analysis against considered observation errors and lumped uncertainties is completed. Finally, the proposed control scheme is verified through experimental tests, and the results show that tracking errors are substantially reduced at low speeds.**

***Index Terms*—Cogging torque, periodic harmonic, permanent-magnet dc (PMDC) torque motor, reduced-order nonlinear observer (RONO), speed control, triple-step nonlinear method.**

I. Introduction

PERMANENT-MAGNET dc (PMDC) motors continue to be widely used for mechanical or electrical propulsion in motion control systems. When these motors are applied as direct drive devices in an automated guided vehicle (AGV) [1], precise control of full-speed range, especially low-speed precise control, becomes a challenging issue. In low-speed condition, cogging torque and friction torque deserve special mention because of the significant influence on speed control.

Cogging torque is an undesirable disturbance and results in speed ripple. It is especially prominent at lower speeds, with the symptom of jerkiness. Reduction in cogging torque can be achieved by implementing appropriate design techniques for PM motors [2]. Moreover, modern microprocessors permit developing disturbance-observer-based control methods [3]–[5] to compensate for the cogging torque disturbance, which is implemented virtually with no extra cost. If the cogging torque is considered as a slow time-varying disturbance, it can be estimated by many methods, such as extended state observer (ESO) [6], [7], Luenberger observer [8], [9] and nonlinear disturbance observer [10], [11]. In [12], torque ripples are rejected by coupling a load torque observer with a torque feed-forward loop. In addition, considering that the cogging torque changes harmonically, the cogging torque is a fast time-varying disturbance. Since the performance of ESO is not satisfactory for estimating a fast-varying disturbance, a higher order ESO is expected to offer improvements in [13]. A nonlinear observer was designed in [14] to estimate harmonic disturbance with known frequency and unknown amplitude and phase. Based on the dynamics of periodic disturbance (an undamped second-order system), a Luenberger state observer was properly designed in [15] to compensate periodic torque disturbances. In [16], a proportional–integral (PI) controller combined with a harmonic disturbance estimator was used to improve speed regulation performance for a dc motor. The assumption of constant or slowly varying speed is used or implied in analysis.

In low-speed condition, friction torque has a significant impact, with a high degree of nonlinearity [17], [18]. To compensate the friction torque, many dynamic friction models, such as LuGre model [19], 2SEP model [20], GMS model [21], and modified LuGre model [22], are proposed to describe the friction phenomena. Among them, a continuous and differentiable function is employed for LuGre friction model in [22], which is more beneficial for controller design. The friction is also commonly described by static models between velocity and frictional forces. In [23], to facilitate controller implementation, a continuous static–friction model is employed to develop a continuous friction compensation law. An experimental friction map is used to achieve a good control performance in [24].

The AGV system is characterized by nonlinearity, parameter variations, and unknown disturbances [25]. Conventional

Manuscript received September 30, 2015; revised March 5, 2016, May 15, 2016, and June 23, 2016; accepted July 12, 2016. Date of publication August 4, 2016; date of current version March 8, 2017. This work was supported in part by the 973 Program under Grant 2012CB821202, and in part by the National Natural Science Foundation of China under Grant 61520106008 and Grant 61522307. *(Corresponding author: Hong Chen.)*

H. Chu, W. Gu, and H. Chen are with the State Key Laboratory of Automotive Simulation and Control, Jilin University, Changchun 130022, China, and also with the Department of Control Science and Engineering, Jilin University, Changchun 130025, China (e-mail: chu.hongqing@163.com; guwanli888@163.com; chenh@jlu.edu.cn).

B. Gao is with the State Key Laboratory of Automotive Simulation and Control, Jilin University, Changchun 130022, China (e-mail: gaobz@jlu.edu.cn).

Color versions of one or more of the figures in this paper are available online at http://ieeexplore.ieee.org.

Digital Object Identifier 10.1109/TIE.2016.2598298

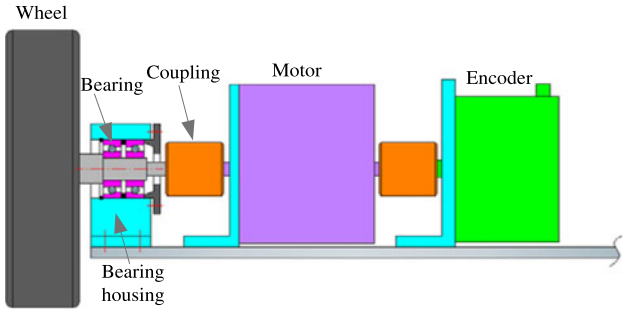

Fig. 1. Schematic of the AGV drives.

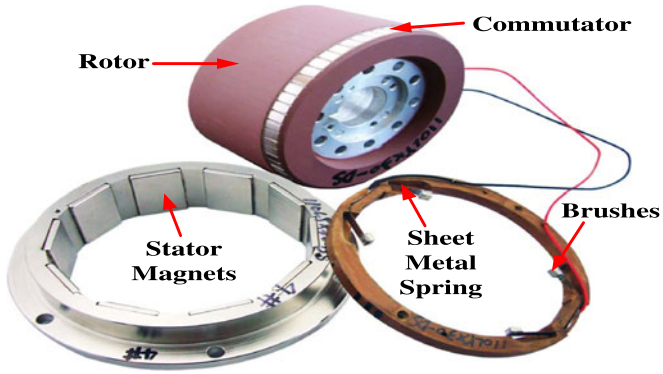

Fig. 2. PMDC torque motor.

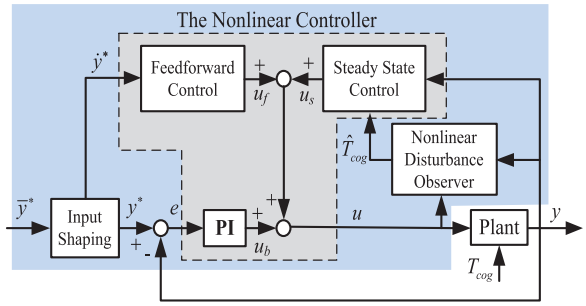

Fig. 3. Diagram of the nonlinear-disturbance-observer-based control scheme.

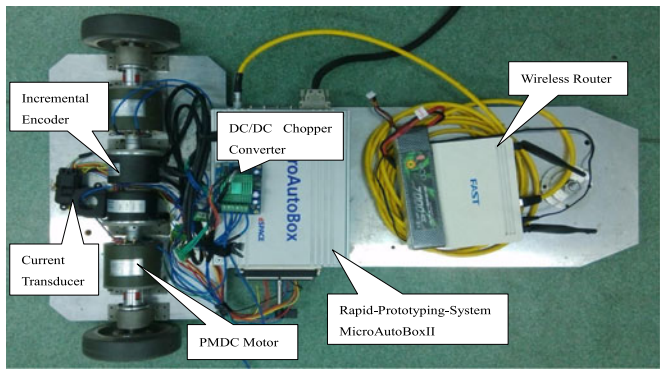

Fig. 4. Experimental setup.

linear control methods, such as PID control, cannot guarantee a sufficiently high performance [26]–[28]. To enhance control performance, a considerable number of modern control methods have been developed for PMDC motors, including sliding mode control [29], model reference adaptive control [30], observer-based robust control [31], and triple-step nonlinear method [24]. Each of them has its own characteristics and has also been effectively implemented. The triple-step nonlinear method can avoid a amount of complex derivation and tolerate the experimental map in the process of controller design [24], [32].

This paper provides a novel disturbance observer-based nonlinear triple-step controller to improve the low-speed tracking performance for the PMDC motor. First, to model the fast varying properties of cogging torque, a nonlinear parameter-varying high-order system is established. Second, based on the nonlinear parameter-varying high-order system, a reduced-order nonlinear observer (RONO) is designed to estimate the cogging torque, and the robustness analysis with regard to the uncertainties is completed. It is worth noting that the robustness analysis does not require the assumption of constant or slowly varying speed. Third, a triple-step nonlinear method is applied to derive a speed tracking controller, wherein two disturbance inputs, namely the observation errors and lumped uncertainties, are considered. Finally, to verify the performance of proposed control scheme, main experimental results, including observation results, compensation results, and comparative results, are obtained for the PMDC motor.

The rest of the paper is organized as follows. Section II presents a nonlinear dynamic model of the PMDC motor in AGV. In Section III, a RONO is designed to estimate the cogging torque. Then, an observer-based controller is constructed using a triple-step nonlinear method in Section IV. The main experimental results, including observation results, compensation results, and comparative results, are presented in Section V, and finally the conclusions are provided in Section VI.

II. System Modeling

The AGV drives, as shown in Fig. 1, adopt a PMDC torque motor as the power source because of its high torque output. The PMDC torque motor, as shown in Fig. 2, has many commutator segments placed on the motor rotor. Brushes are forced on the commutator segments by sheet metal springs. PMs are mounted in inner periphery of motor stator. A current-carrying rotor is placed inside the magnetic field to produce mechanical force.

The most common dynamic model of this drive system consists of voltage balance equation

$$L_a \dot{i}_a = V_{\rm bat} u - R_a i_a - k_v \omega \tag{1}$$

and torque balance equation

$$J_m \dot{\omega} = k_t i_a - T_{\rm ml} - T_{\rm fmap}(\omega) - T_{\rm cog} \tag{2}$$

where L_a is the armature inductance, i_a is the armature current, $V_{\rm bat}$ is the input dc voltage, u is the chopper duty cycle, R_a is the armature resistance, k_v is the back EMF coefficient, ω is the motor shaft rotational speed, J_m is the overall equivalent moment of inertia, k_t is the torque constant, $T_{\rm ml}$ is the load torque, $T_{\rm fmap}(\omega)$ is the friction torque of the motor and bearings, and $T_{\rm cog}$ is the cogging torque.

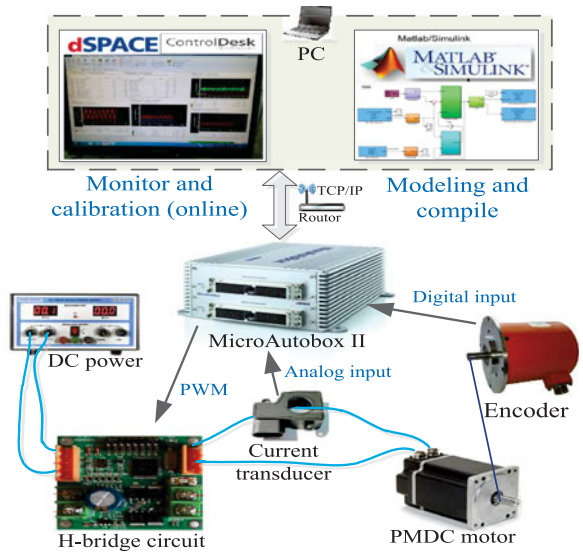

Fig. 5. Implementation architecture.

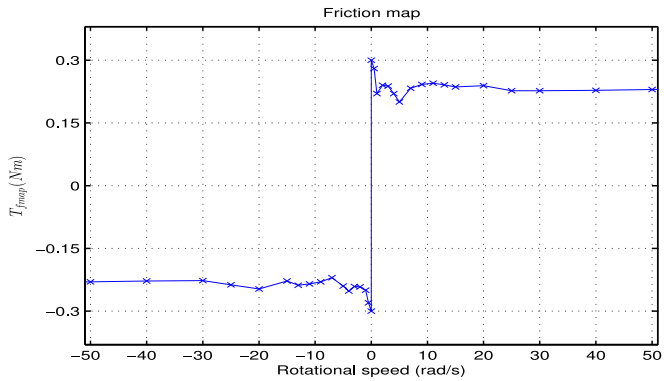

Fig. 6. Friction map.

The main driving condition is a flat road for the AGV in this paper, thus the nominal load torque $T_{\rm ml}$, which is mainly from rolling resistance, can be considered as a known variable. Despite that a slight bias will exist in the nominal load torque inevitably, it is acceptable in applications according to the robustness analyses of the proposed observer and controller (given in Sections III and IV).

The friction torque $T_{\rm fmap}(\omega)$ is a function of the motor speed. Due to the complexity of friction, the friction is most commonly described by a lookup table in industrial applications [33]. To keep the original form of experimental data and make the friction more accurate, the friction is presented by an experimental map, as shown in Fig. 6.

The cogging torque in PMDC motor results from the contact force between brushes and commutator segments, from the switching action and sometimes from the bearings. It is undesirable but inevitable in PM motor [2], [34]. In general, the periodic cogging torque can be decomposed into the sum of a finite order of harmonics. Each order harmonic of the cogging torque can be represented by a time-domain solution of an undamped second-order system [15], [16]. For instance, the time-domain solution of the ith torque harmonic is presented as

$$\ddot{T}_{\rm cog}(i) + (\lambda_{\rm i}\omega)^2 T_{\rm cog}(i) = 0,\ i = 1, 2, \ldots, k \tag{3}$$

where $\lambda_{\rm i}$ is the fundamental frequency of the ith torque harmonic. Fundamental frequency is determined by the motor mechanical structure, which can be acquired through signal processing, $\lambda_{\rm i} = i\lambda_1$, for $\forall i \neq j, \lambda_i \neq \lambda_j$. For the second-order system (3), by introducing state variables ξ_{2i-1}, ξ_{2i}, the model of the ith torque harmonic is written as

$$\begin{aligned} \dot{\xi}_{2i-1} &= \xi_{2i} \\ \dot{\xi}_{2i} &= -(\lambda_{\rm i}\omega)^2 \xi_{2i-1} \\ T_{\rm cog}(i) &= \xi_{2i-1}. \end{aligned} \tag{4}$$

Then, the cogging torque is represented as follows:

$$\dot{\xi} = A(\omega)\xi \tag{5a}$$

$$T_{\rm cog} = C\xi \tag{5b}$$

where $A(\omega) = \begin{bmatrix} 0 & 1 & \cdots & 0 & 0 \\ -(\lambda_1\omega)^2 & 0 & \cdots & 0 & 0 \\ \vdots & \vdots & \ddots & \vdots & \vdots \\ 0 & 0 & \cdots & 0 & 1 \\ 0 & 0 & \cdots & -(\lambda_{\rm k}\omega)^2 & 0 \end{bmatrix}$, $\xi = \begin{bmatrix} \xi_1 & \xi_2 & \ldots & \xi_{2k-1} & \xi_{2k} \end{bmatrix}^T$, $C = \begin{bmatrix} 1 & 0 & \ldots & 1 & 0 \end{bmatrix}$.

In this drive system, a H-bridge circuit including four MOSFETs is used as a dc/dc chopper converter, and a very high-switching frequency, such as 10 KHz, is set to ensure that no noticeable dither exists in the armature current. In addition, compared to motor's mechanical time constant, the electrical time constant is small when regulating the chopper duty cycle [35], namely $\frac{L_a}{R_a} \approx 0$. Therefore the left-hand side of (1) can be assumed as zero in the speed control cycle, and (1) is simplified as

$$i_a = \frac{V_{\rm bat}u - k_v\omega}{R_a}. \tag{6}$$

By substituting (6) into (2), the torque balance equation of the AGV drives becomes

$$\dot{\omega} = -\frac{k_t k_v}{J_m R}\omega + \frac{k_t V_{\rm bat}}{J_m R}u - \frac{T_{\rm fmap}(\omega)}{J_m} - \frac{T_{\rm ml}}{J_m} - \frac{T_{\rm cog}}{J_m}. \tag{7}$$

The output to be controlled for the AGV drives is the motor rotational speed, i.e., $y = \omega$, and the reference speed trajectory y^* is commonly provided by an upper optimization algorithm. Based on (5) and (7), the dynamic model is summarized in the following representation for the AGV drives:

$$\dot{\omega} = b_1\omega + b_2 u + b_3(T_{\rm fmap}(\omega) + T_{\rm ml} + C\xi) \tag{8a}$$

$$\dot{\xi} = A(\omega)\xi \tag{8b}$$

$$y = \omega \tag{8c}$$

where $b_1 = -\frac{k_t k_v}{J_m R}$, $b_2 = \frac{k_t V_{\rm bat}}{J_m R}$, $b_3 = -\frac{1}{J_m}$.

The system (8) contains an undifferentiable item $T_{\rm fmap}(\omega)$, as shown in Fig. 6, which is undesirable for controller design [22]. Since the varying parameter ω appears nonlinearly in the matrix $A(\omega)$, the system (8) is a nonlinear parameter-varying high-order system. When ω is constant, the cogging torque generated by (8b) is known as a fixed-frequency periodic disturbances, as in [3], [14]. However, ω is time-varying in practice, which

makes many linear methods used in [15], [16] no longer applicable to stability analysis. For clarity of control scheme, it is reasonable to consider that cogging torque is generated by the exogenous system (8b), then a disturbance observer-based control scheme is employed to achieve good tracking performance. In the following, a RONO is designed to estimate the internal states ξ, and then the speed tracking controller is derived by the triple-step nonlinear method.

III. RONO for Cogging Torque

A. Reduced-Order Observer Design

To estimate the unmeasured cogging torque, the RONO is designed properly. Based on the augmented model (8b), the RONO can be designed in the following form:

$$\dot{\hat{\xi}} = A(\omega)\hat{\xi} + L(\omega)[\dot{\omega} - b_1\omega - b_2 u - b_3(T_{\mathrm{fmap}}(\omega) + T_{\mathrm{ml}} + C\hat{\xi})] \tag{9}$$

where $L(\omega) \in \mathbb{R}^{2k\times 1}$ is the gain to be determined and allowed to be dependent on ω.

Defining the estimation error as $e_\xi = \xi - \hat{\xi}$, we then obtain the error dynamics as follows:

$$\dot{e}_\xi = \dot{\xi} - \dot{\hat{\xi}} = [A(\omega) - L(\omega)b_3 C]e_\xi = -\begin{bmatrix} l_1(\omega)b_3 & -1 & \cdots & l_1(\omega)b_3 & 0 \\ l_2(\omega)b_3 + (\lambda_1\omega)^2 & 0 & \cdots & l_2(\omega)b_3 & 0 \\ \vdots & \vdots & \ddots & \vdots & \vdots \\ l_{2k-1}(\omega)b_3 & 0 & \cdots & l_{2k-1}(\omega)b_3 & -1 \\ l_{2k}(\omega)b_3 & 0 & \cdots & l_{2k}(\omega)b_3 + (\lambda_{\mathrm{k}}\omega)^2 & 0 \end{bmatrix} e_\xi. \tag{10}$$

For all rotational speeds $\omega \neq 0$, under the condition $\forall\ i \neq j$, $\lambda_{\mathrm{i}} \neq \lambda_{\mathrm{j}}$, if the observer gain

$$L(\omega) = \begin{bmatrix} l_1(\omega) & l_2(\omega) & \cdots & l_{2k-1}(\omega) & l_{2k}(\omega) \end{bmatrix}^T \tag{11}$$

can be properly selected such that (11) is globally exponentially stable regardless of ω, the RONO (10) can exponentially track the cogging torque [3].

The observer gain is suggested as

$$L(\omega) = \begin{bmatrix} \frac{1}{b_3}m_1 \\ \frac{1}{b_3}(m_2 - (\lambda_1\omega)^2) \\ \vdots \\ \frac{1}{b_3}m_{2k-1} \\ \frac{1}{b_3}(m_{2k} - (\lambda_k\omega)^2) \end{bmatrix} \tag{12}$$

where ω^2 is bounded with regard to the low-speed control for the PMDC motor. Then, the error dynamics becomes

$$\begin{aligned} \dot{e}_\xi &= -\begin{bmatrix} m_1 & -1 & \cdots & m_1 & 0 \\ m_2 & 0 & \cdots & m_2 - \lambda_1^2\omega^2 & 0 \\ \vdots & \vdots & \ddots & \vdots & \vdots \\ m_{2k-1} & 0 & \cdots & m_{2k-1} & -1 \\ m_{2k} - \lambda_{\mathrm{k}}^2\omega^2 & 0 & \cdots & m_{2k} & 0 \end{bmatrix} e_\xi \\ &= -\begin{bmatrix} m_1 & -1 & \cdots & m_1 & 0 \\ m_2 & 0 & \cdots & m_2 & 0 \\ \vdots & \vdots & \ddots & \vdots & \vdots \\ m_{2k-1} & 0 & \cdots & m_{2k-1} & -1 \\ m_{2k} & 0 & \cdots & m_{2k} & 0 \end{bmatrix} e_\xi \\ &\quad -\begin{bmatrix} 0 & 0 & \cdots & 0 & 0 \\ 0 & 0 & \cdots & -\lambda_1^2 & 0 \\ \vdots & \vdots & \ddots & \vdots & \vdots \\ 0 & 0 & \cdots & 0 & 0 \\ -\lambda_{\mathrm{k}}^2 & 0 & \cdots & 0 & 0 \end{bmatrix} e_\xi\omega^2 := -Me_\xi - Ne_\xi\omega^2. \end{aligned} \tag{13}$$

In the case of $k = 1$, i.e.

$$M = \begin{bmatrix} m_1 & -1 \\ m_2 & 0 \end{bmatrix}, \quad N = 0. \tag{14}$$

The characteristic equation of the error dynamics is obtained as follows:

$$\det(sI - (-M)) = s^2 + m_1 s + m_2 = 0. \tag{15}$$

If $m_1 > 0, m_2 > 0$, and $m_2 \neq \lambda_1^2\omega^2$, each eigenvalue or characteristic root of the error dynamics has strictly negative real part, and then the error dynamics is globally exponentially stable.

For the case of $k \geq 2$, a Lyapunov function for the proposed observer is given as

$$V_{\mathrm{o}} = e_\xi^T P e_\xi \tag{16}$$

and differentiate it along the observer error dynamics (13) to obtain

$$\begin{aligned} \dot{V}_{\mathrm{o}} &= \dot{e}_\xi^T P e_\xi + e_\xi^T P \dot{e}_\xi \\ &= -e_\xi^T(M^T P + PM)e_\xi - e_\xi^T(N^T P + PN)e_\xi\omega^2. \end{aligned} \tag{17}$$

If there exist $m_1, m_2 \ldots m_{2k}$ and symmetric matrix P such that

$$M^T P + PM > 0 \tag{18a}$$

$$N^T P + PN > 0 \tag{18b}$$

$$P > 0 \tag{18c}$$

the observer error dynamics is exponentially stable.

The search for symmetric matrix P and variables m_1, $m_2 \ldots m_{2k}$ that satisfy the inequalities (18) is a Bilinear Linear

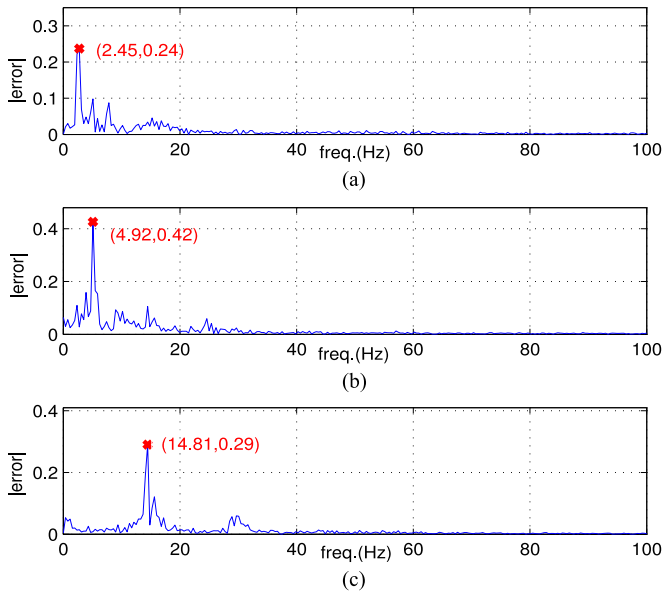

Fig. 7. Amplitude spectra of speed tracking error using triple-step nonlinear method.

Matrix Inequalities (BMIs) feasibility problem [36]. The solution to inequalities (18) can be implemented by the BMI solver proposed in [37]. The BMI solver is a MATLAB package for solving optimization problems with BMI constraints.

B. Implementation Issues

Differentiation of the measurement signal is not a recommended operation in the observer implementation since it is sensitive to noise. An appropriate transformation of variables can be used to avoid the differentiation of the measurement signal. Following the idea, for example, in [3] and [4], we define the transformation of

$$\eta = \hat{\xi} - P(\omega) \tag{19}$$

where $P(\omega) = \begin{bmatrix} p_1(\omega) & p_2(\omega) & \dots & p_{2k-1}(\omega) & p_{2k}(\omega) \end{bmatrix}^T$. By the differentiation operation, we infer

$$\dot{\eta} = [A(\omega) - L(\omega)b_3C]\hat{\xi} - L(\omega)\left[b_1\omega + b_2u + b_3(T_{\text{fmap}}(\omega) + T_{\text{ml}})\right] + \left[L(\omega) - \frac{\partial P(\omega)}{\partial \omega}\right]\dot{\omega}. \tag{20}$$

With the choice of $P(\omega)$ as

$$L(\omega) = \frac{\partial P(\omega)}{\partial \omega} \tag{21}$$

we arrive at

$$\dot{\eta} = [A(\omega) - L(\omega)b_3C]\hat{\xi} - L(\omega)[b_1\omega + b_2u + b_3(T_{\text{fmap}}(\omega) + T_{\text{ml}})]. \tag{22}$$

Hence, (22), together with (19) and (21) represents the designed observer that can be implemented.

It can be seen from the amplitude spectra analysis of speed tracking error, as shown in Fig. 7, the most significant torque harmonic is the first-order one.

In the case of $k = 1$, to satisfy the relationship of (21), i.e.

$$l_1(\omega) = \frac{\partial p_1(\omega)}{\partial \omega}, \quad l_2(\omega) = \frac{\partial p_2(\omega)}{\partial \omega} \tag{23}$$

the auxiliary variables are given by $p_1(\omega) = \frac{m_1}{b_3}\omega$, $p_2(\omega) = \frac{m_2\omega - \frac{1}{3}\lambda_1^2\omega^3}{b_3}$.

C. Robustness Analysis of Observer

From the application point of view, there are some biases between the values of the nominal parameters and the actual parameters in real system, and compared to their actual value the friction and load torque have some gap. It is reasonable to add a bounded d to represent the uncertainties. Equation (8a) is written as

$$\dot{\omega} = b_1\omega + b_2u + b_3(T_{\text{fmap}}(\omega) + T_{\text{ml}} + C\xi) + d \tag{24}$$

where $d = \delta b_1\omega + \delta b_2u + \delta b_3(\delta T_{\text{fmap}}(\omega) + \delta T_{\text{ml}})$. δ is difference operator which denotes uncertainty in a physical parameter. The error dynamics is then described by

$$\dot{e}_\xi = [A(\omega) - L(\omega)b_3C]e_\xi - L(\omega)d \tag{25}$$

where $L(\omega)$ in (12) is bounded with regard to the low-speed control. For the case of $k \geq 2$, the derivative of the Lyapunov function becomes

$$\dot{V}_{\text{o}} = -e_\xi^T(M^TP + PM)e_\xi - e_\xi^T(N^TP + PN)e_\xi\omega^2 - L(\omega)^TdPe_\xi - e_\xi^TPL(\omega)d. \tag{26}$$

Using Young's Inequality [38], the above equality becomes

$$\dot{V}_{\text{o}} \leq -e_\xi^T(M^TP + PM)e_\xi - e_\xi^T(N^TP + PN)e_\xi\omega^2 + \kappa_1e_\xi^Te_\xi + \frac{d^2}{4\kappa_1}L(\omega)^TP^2L(\omega) + \kappa_2e_\xi^Te_\xi + \frac{d^2}{4\kappa_2}L(\omega)^TP^2L(\omega) \tag{27}$$

where $\kappa_1 > 0$ and $\kappa_2 > 0$. Appropriate P and $m_1, m_2 \dots m_{2k}$ satisfy the following inequality:

$$\begin{aligned} M^TP + PM - \kappa_1 - \kappa_2 &> 0 \\ N^TP + PN &> 0 \\ P &> 0 \end{aligned} \tag{28}$$

then the error dynamics is input-to-state stable (ISS) with regard to the considered uncertainties d (see [38, p. 503]). Note that the above analysis does not require the assumption of constant or slowly varying speed. The search for symmetric matrix P and variables $m_1, m_2 \dots m_{2k}$ that satisfy the inequalities (28) is a BMIs feasibility problem.

Similarly, for the case of $k = 1$, the observer system is also ISS.

IV. Observer-Based Nonlinear Controller Design

In this section, the speed tracking controller is derived by the triple-step nonlinear method for the PMDC torque motor. From the perspective of engineering applications, each design step of

triple-step method has different engineering purposes. As a result, the derived control law has a clear form, which benefits for application engineers to understand the engineering purpose of each part in control law. The design procedure consists of three steps, namely steady-state-like control, reference-dynamics-based feedforward control, and error feedback control.

A. Step 1: Steady-State-Like Control

If the system is in steady state, it is reasonable to let $\dot{y} = 0$. By substituting it into (8a), the steady-state control law can be obtained as follows:

$$u_s = -\frac{1}{b_2}[b_1\omega + b_3(T_{\mathrm{fmap}}(\omega) + T_{\mathrm{ml}} + C\xi)]. \tag{29}$$

The steady-state control law (29) is the dominant control action which contains the cogging torque, the experimental friction map, the load torque, and the state-dependent item.

B. Step 2: Reference-Dynamics-Based Feedforward Control

It is clear that only a steady-state control is not enough to achieve satisfying performance. Some additional information such as reference variations of the control system should be considered. Hence, the additional input u_f is added, and the control input is adjusted to the following form:

$$u = u_s + u_f \tag{30}$$

where u_s is given by (29), u_f is to be determined. By substituting (29) and (30) into (8a), the system dynamics can be represented as

$$\dot{y} = b_2 u_f. \tag{31}$$

Note that the clear form of (31) benefits from the steady-state control law (29).

Then, by enforcing $\dot{y} = \dot{y}^*$ for (31), the reference-dynamics-related control law is obtained as follows:

$$u_f = \frac{1}{b_2}\dot{y}^*. \tag{32}$$

The obtained u_f contains the reference dynamics $\dot{y}^*$, hence it can be considered as a reference-dynamics-related control law.

C. Step 3: Error Feedback Control

In the aforementioned two steps, the tracking error is not considered. To deal with the final tracking error and achieve better tracking performance, a new control action u_b is introduced, then the control input is changed into the form

$$u = u_s + u_f + u_b \tag{33}$$

where u_s is given by (29), u_f is given by (32), and u_b is to be determined. By substituting (29), (32), and (33) into (8a), the system dynamics can be presented as

$$\dot{y} = \dot{y}^* + b_2 u_b. \tag{34}$$

Then, by defining the tracking error as $e_1 = y^* - y$, the output error dynamics is obtained as

$$\dot{e}_1 = -b_2 u_b. \tag{35}$$

For the error system given in (35), a Lyapunov function is selected as

$$V_{\mathrm{c}} = \frac{1}{2}r^2 \tag{36}$$

where $r = e_1 + \alpha\chi, \chi = \int e_1 dt, \alpha > 0$ and its derivative with respect to time is

$$\dot{V}_{\mathrm{c}} = r\dot{r} = (e_1 + \alpha\chi)(-b_2 u_b + \alpha e_1). \tag{37}$$

By enforcing $-b_2 u_b + \alpha e_1 = -\frac{\kappa}{2}(e_1 + \alpha\chi)$, if $\kappa > 0$, then $\dot{V}_{\mathrm{c}} = -\frac{\kappa}{2}(e_1 + \alpha\chi)^2 < 0$, and the control system is asymptotically stable. Hence, the error feedback control law is obtained as follows:

$$u_b = \frac{1}{b_2}\left[\left(\alpha + \frac{\kappa}{2}\right)e_1 + \frac{\kappa\alpha}{2}\chi\right]. \tag{38}$$

Note that, with the help of the steady-state control law (29) and the reference-dynamics-related control law (32), the output error dynamics is obtained as a clear form. Furthermore, the error feedback control law is obtained easily.

By combining (29) and (32) with (38), the entire control law is provided as follows:

$$\begin{aligned} u =& \ u_s + u_f + u_b \\ =& -\frac{1}{b_2}[b_1\omega + b_3(T_{\mathrm{fmap}}(\omega) + T_{\mathrm{ml}} + C\xi)] \\ &+ \frac{1}{b_2}\dot{y}^* + k_{\mathrm{p}}e_1 + k_{\mathrm{i}}\chi \end{aligned} \tag{39}$$

where $k_{\mathrm{p}} = \frac{1}{b_2}(\alpha + \frac{\kappa}{2}), k_{\mathrm{i}} = \frac{\kappa\alpha}{2b_2}$.

D. Implementation Issues

The state ξ is unmeasured in (39) and substituted by its observation $\hat{\xi}$ during implementation. Hence, the entire implementation-oriented control law becomes

$$\begin{aligned} u_{\mathrm{im}} =& -\frac{1}{b_2}[b_1\omega + b_3(T_{\mathrm{fmap}}(\omega) + T_{\mathrm{ml}} + C\hat{\xi})] \\ &+ \frac{1}{b_2}\dot{y}^* + k_{\mathrm{p}}e_1 + k_{\mathrm{i}}\chi. \end{aligned} \tag{40}$$

The input shaping technique [39], [40] can protect the system from damage resulting from a sudden change in the command signal. In this paper, the input shaping filter is

$$\frac{y^*}{\bar{y}^*} = \frac{1}{\tau s + 1} \tag{41}$$

wherein the choice of time constant τ depends on limited bandwidth of the reference signal.

The proposed observer-based nonlinear controller has a concise structure, which is shown in Fig. 3. The steady-state-like control u_s is the dominant control action, which contains the observed cogging torque, the experimental friction map, the load torque, and the state-dependent item. The feedforward control

u_f helps to improve transient tracking performance by using the information of reference dynamics. The error feedback control u_b is derived by solving a differentiable control-Lyapunov function, which makes it possible to guide gain calibration to reduce controller calibration work.

E. Robustness Analysis of Controller

In the implementation-oriented control law (40), the state ξ is substituted by observation $\hat{\xi}$, which brings the observer error e_ξ into the system input. In addition, due to the gap between the real friction and the obtained friction map, it is reasonable to introduce the bounded Δ as lumped uncertainties. Then, we have

$$u = u_{\text{im}} - \frac{b_3}{b_2} C e_\xi + \Delta. \tag{42}$$

Substituting the implementation-oriented control law (40) into system (8a), the closed-loop error system (35) with disturbance observer error becomes

$$\dot{e}_1 = -\left(\alpha + \frac{\kappa}{2}\right) e_1 - \frac{\kappa\alpha}{2}\chi - b_3 C e_\xi + b_2 \Delta. \tag{43}$$

Thus, the derivative of V_{c} provided in (36) becomes

$$\dot{V}_{\text{c}} = -\frac{\kappa}{2}(e_1 + \alpha\chi)^2 - b_3 C e_\xi (e_1 + \alpha\chi) + b_2 \Delta (e_1 + \alpha\chi). \tag{44}$$

Applying Young's Inequality [38] to the last two terms of the above equality leads to

$$\begin{aligned} -b_3 C e_\xi (e_1 + \alpha\chi) &\le \frac{1}{2}(b_3 C e_\xi)^2 + \frac{1}{2}(e_1 + \alpha\chi)^2 \\ b_2 \Delta (e_1 + \alpha\chi) &\le \frac{1}{2}(b_2 \Delta)^2 + \frac{1}{2}(e_1 + \alpha\chi)^2. \end{aligned} \tag{45}$$

Then, (44) becomes

$$\dot{V}_{\text{c}} \le -\frac{\kappa - 2}{2}(e_1 + \alpha\chi)^2 + \frac{1}{2}(b_3 C e_\xi)^2 + \frac{1}{2}(b_2 \Delta)^2. \tag{46}$$

According to the robustness analysis of observer in Section III-C, the observer error dynamics admits ISS property with respect to the considered uncertainties d. If $\kappa > 2$, according to [38, Lemma C.5, Remark C.6, p. 506], the entire controller system is ISS with respect to two inputs: the uncertainties Δ and the observer error e_ξ.

According to [38, p. 505], the complete system can easily establish ISS property by the ISS-Lyapunov functions V_{o} and V_{c}.

V. Experimental Results

The AGV experimental setup, which is shown in Fig. 4, consists of PMDC torque motor, high-precision incremental encoder (with 65 535 counts per revolution), current transducer (LEM, with linearity error of 1%), wireless router (with data transfer rate of 100 Mb/s), commercial dc/dc chopper converter (H-bridge circuit with 10 KHz switching frequency), and rapid-prototyping-system MicroAutoBoxII (with PPC750 GL Power PC processor, 900 MHz clock frequency, 24 MB RAM, and 16-b resolution for analog input). The nominal values of system parametersare shown in Table I. According to Fig. 5, the implementation process is summarized as follows.

TABLE I
Nominal Parameters in the AGV Drives

k_v	Back EMF coefficient	$0.153\,\text{V}/(\text{rad/s})$
k_t	Torque coefficient	$0.125\,\text{N}\cdot\text{m/A}$
V_{bat}	Battery voltage	$12\,\text{V}$
J_m	Inertia	$3.5 \times 10^{-3}\,\text{kg}\cdot\text{m}^2$
R_a	Internal resistance	1Ω

Step 1: Determine sampling interval. After I/O ports designation for the incremental encoder, frequency method is provided to determine motor rotational speed by MicroAutoBoxII. According to speed measurement tolerance at low-speed condition, the system sampling interval is set as 5 ms.

Step 2: Establish the proposed observer-based controller in MATLAB/Simulink, as shown in light-blue part of Fig. 3, and complete model configurations for real-time implementation, such as configuring fixed-step solver ($ode3$) and variable's data type (Boolean, double, etc.), variable initialization.

Step 3: Transform the established observer-based-controller model into real-time C source code using Embedded Coder and then download it on MicroAutoBoxII.

Step 4: Monitor signals and calibrate the gains by using hardware-management software ControlDesk.

This paper especially focuses on the compensation of the periodic cogging torque. To better illustrate the performance of the proposed scheme, the load torque is set to zero in experiments. The friction map $T_{\text{fmap}}(\omega)$, which is shown in Fig. 6, is calibrated through steady-state experiments. The average value of the periodic cogging torque is zero for one complete revolution of the rotor. As described in the torque balance (2), in steady-state and no-load condition, the average value of the friction equals to the average value of the armature torque for one complete revolution of the rotor, which means that the friction under different rotational speeds can be obtained by measuring the average value of the armature current. Note that it is necessary to perform several groups of experiments to obtain more accurate value at lower speeds.

A. Fundamental Frequency Analysis

The fundamental frequency of the torque harmonic is obtained before validating the proposed observer. Steady-state tracking experiments are carried out using the proposed implementation-oriented control law (40). But the observation $\hat{\xi}$ is replaced by 0 here. The reference rotational speeds are set to 0.5, 1, and 3 rad/s. The impact of cogging torque on the output rotational speeds is effectively shown in the tracking error, and the information on cogging torque frequency can be extracted directly from it. The tracking error is converted from the time domain to the frequency domain through fast Fourier transformation. Then, the amplitude spectra of the tracking error are obtained at 0.5, 1, and 3 rad/s, as shown in Fig. 7. It can be seen from the amplitude spectra in Fig. 7 that the first-order frequency is the most significant. The different orders of frequency can be

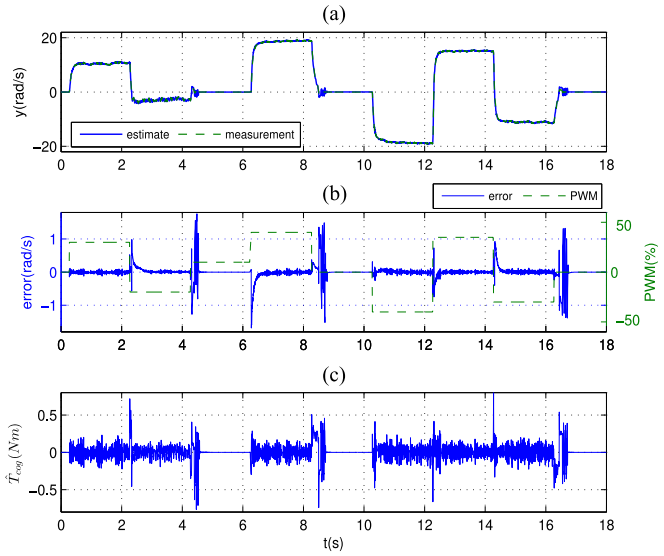

Fig. 8. Observation results in open loop: random input. (a) Estimated and measured velocity, (b) velocity observation error and input (pulse width modulation; PWM), and (c) estimated cogging torque.

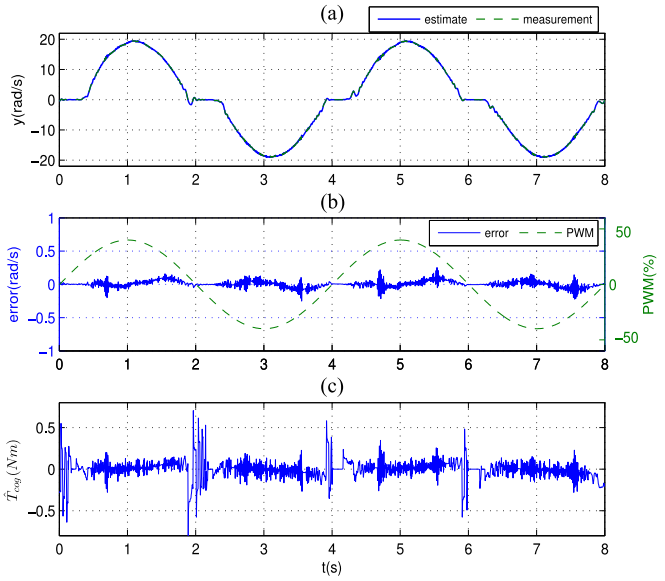

Fig. 9. Observation results in open loop: sine input. (a) Estimated and measured velocity, (b) velocity observation error and input (PWM), and (c) estimated cogging torque.

shown at 0.5, 1, and 3 rad/s. By using the relationship between angular frequency and frequency $\lambda_i\omega = 2\pi f$, the fundamental frequency given in (3) can be obtained as follows:

$$\lambda_1 = 31,\ \lambda_2 = 62, \ldots,\ \lambda_k = 31k. \tag{47}$$

B. Observation Results

To validate the designed cogging-torque observer, the PMDC torque motor in the AGV drives is actuated in an open-loop manner. The same random and sine signals are used as control inputs to two systems: the actual system, the system model with the designed cogging-torque observer. The observer's accuracy is evaluated by comparing the output results between the actual system and the system model.

To compensate the cogging torque in a large extent, the observer gain $L(\omega)$ should be designed to guarantee a fast convergence rate and to reject measurement noises. In implementation of the RONO, according to stability requirement in (15), the gains are selected as follows:

$$l_1(\omega) = -120J_m,\ l_2(\omega) = -J_m\left(115000 - \lambda_1^2\omega^2\right). \tag{48}$$

First, to validate the convergence rate of the RONO, the control input is set as a normally distributed random signal that consists of the sequence of different steps. The observation results are shown in Fig. 8. According to the error between the measured velocity and the estimated velocity in Fig. 8(b) and the estimated cogging torque in Fig. 8(c), the RONO has a fast enough convergence. Noting that, every time the motor direction changes, the observer needs some setting time to converge again. It is evident that the error resulted from friction map in direction changing action influences the cogging torque observation.

Furthermore, to validate the RONO in a varying state, the control input is set as a sine signal. The observation results are shown in Fig. 9. It can be seen from the the error between the measured velocity and the estimated velocity in Fig. 9(b), the observer can estimate practical cogging torque accurately in a varying state.

C. Compensation Results

To evaluate the performance of the proposed scheme in a practical application, compensation of cogging torque is carried out in three different relatively low velocities, namely 0.5, 1, and 3 rad/s. According to the previous design for nonlinear controller in Section IV, the tuning parameters of the proposed implementation-oriented control law are selected as follows.

$$k_p = 173,\ k_i = 286,\ \tau = 0.005. \tag{49}$$

The proposed cogging-torque observer and the implementation-oriented control law (40) are utilized, and the experimental compensation results are shown in Fig. 10. The left-hand side diagrams, (a), (c), and (e), show the tracking performance comparison between cases with and without the proposed observer. The right-hand side diagrams, (b), (d), and (f), show the amplitude spectrum of the corresponding tracking error. As shown in Fig. 10, the tracking errors are substantially reduced by using the above proposed observer. This can be easily recognized in both time and frequency domains.

Compensation of cogging torque is also carried out in continuously changing velocities. The reference velocity signal is set as a sine signal, $y_r = 2 + \sin 1.3t$. The measured experimental results are shown in Fig. 11. As shown in Fig. 11(b), after using the proposed observer, the tracking errors are substantially reduced in continuously changing velocities.

D. Comparative Results

To clearly evaluate the effectiveness of the proposed observer-based controller, under a same reference signal, the comparative

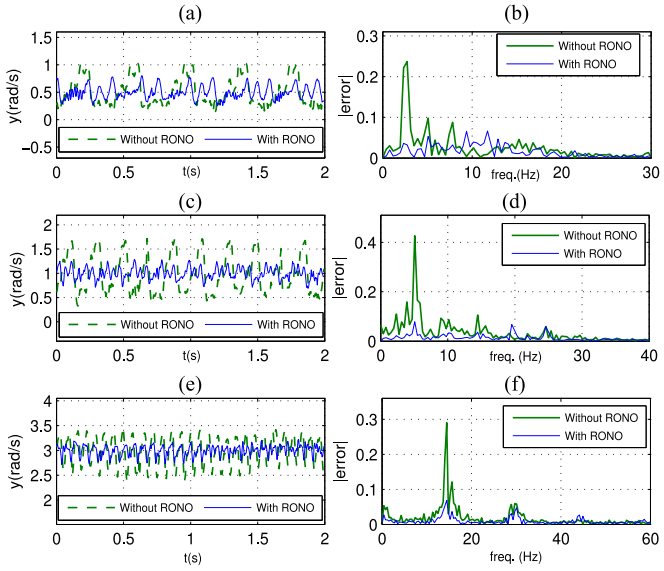

Fig. 10. Experimental results with and without RONO. (a), (c), (e) Tracking 0.5, 1, and 3 rad/s velocities. (b), (d), (f) Amplitude spectrum of the corresponding tracking error.

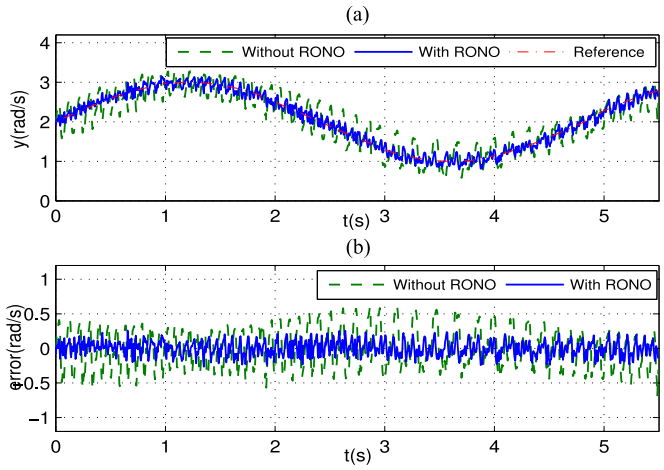

Fig. 11. Experimental results with and without RONO: tracking a sinusoidal signal.

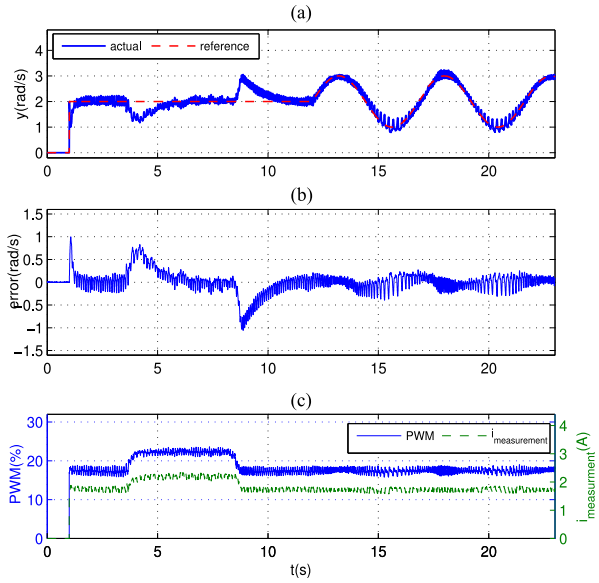

Fig. 12. Experimental tracking performance using the proposed control scheme: (a) rotational speed, (b) tracking error, and (c) control input and measurement current.

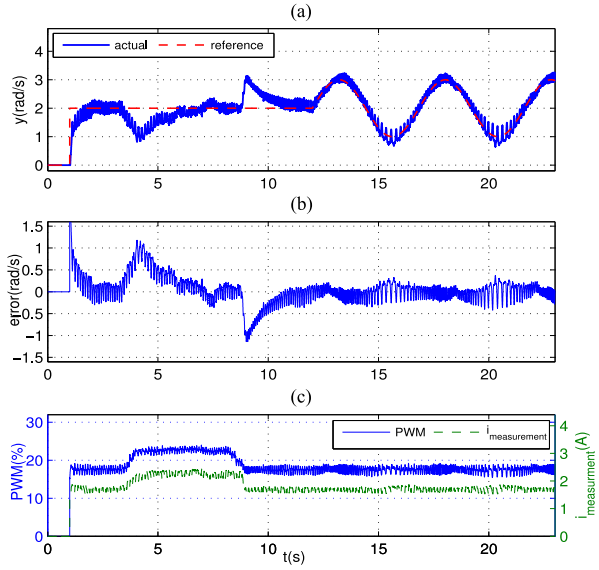

Fig. 13. Experimental tracking performance using PI controller with the proposed observer: (a) rotational speed, (b) tracking error, and (c) control input and measurement current.

experiments are carried out with four control schemes. The four control schemes are as follows.

1) Proposed control scheme: Gains for the proposed observer and the implementation-oriented control law are given in (48) and (49), respectively.

2) PI controller with the proposed observer: Gains for the proposed observer are given in (48) and the PI parameters are chosen as $k_{p1} = 138$, $k_{i1} = 216$.

3) PI controller with an ESO: A new bounded variable $\varepsilon(t)$ is introduced to represent the derivative of cogging torque, i.e., $\dot{T}_{\rm cog} = \varepsilon(t)$. Then, the ESO is designed as

$$\dot{\hat{\omega}} = b_1\hat{\omega} + b_2 u + b_3(T_{\rm fmap}(\hat{\omega}) + T_{\rm ml} + \hat{T}_{\rm cog}) + h_1(\omega - \hat{\omega})$$

$$\dot{\hat{T}}_{\rm cog} = h_2(\omega - \hat{\omega})$$

where h_1, h_2 are the observer gains to be determined. In implementation of this control scheme, the observer gains are chosen as $h_1 = 84$, $h_2 = 376$, and PI parameters are chosen as $k_{p2} = 103$, $k_{i2} = 171$.

4) Double-loop PID controller: The well-tuned PID parameters for outer loop and inner loop are chosen as $k_{\rm pout} = 73$, $k_{\rm iout} = 58$; $k_{\rm pin} = 106$, $k_{\rm iin} = 12$.

The corresponding experimental results are, respectively, shown in Figs. 12–15. The reference signals consist of a step signal and a sine signal. The comparison of tracking error under different control schemes is given in Table II, wherein maximal absolute values of the tracking errors are evaluated. It can be concluded that the tracking performance of the proposed control scheme is better than that of the other three control schemes.

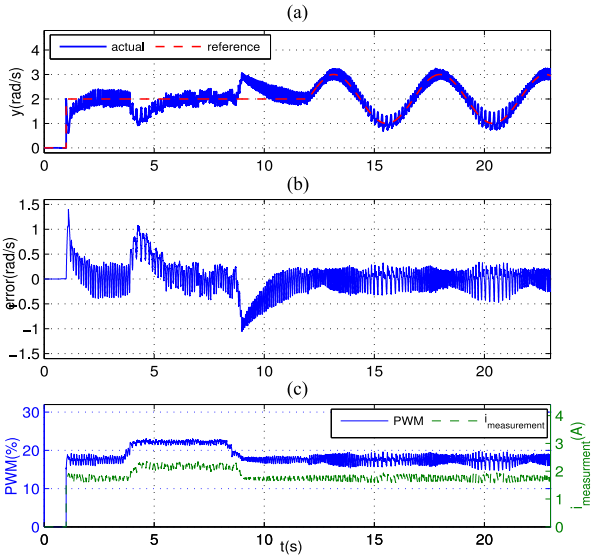

Fig. 14. Experimental tracking performance using PI controller with an ESO: (a) rotational speed, (b) tracking error, and (c) control input and measurement current.

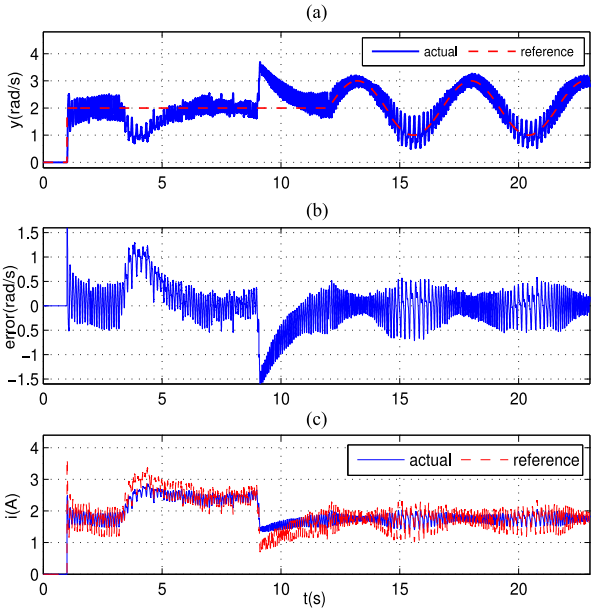

Fig. 15. Experimental tracking performance using well-tuned double-loop PID controller: (a) rotational speed, (b) tracking error, and (c) current response in inner loop.

TABLE II
TRACKING ERROR COMPARISON

Controller		$y=2$ Max$\|e\|$ (rad/s)	$y=2+\sin 1.3t$ Max$\|e\|$ (rad/s)
Proposed control scheme	Nominal value (*)	0.21	0.35
	$J_m = 0.8J_m^*$	0.21	0.39
	$T_{\mathrm{fmap}} = 1.2T_{\mathrm{fmap}}^*$	0.24	0.41
	$J_m, T_{\mathrm{fmap}} = 1.2(*)$	0.22	0.38
PI+RONO		0.25	0.42
PI+ESO		0.39	0.45
Double-loop PID		0.50	0.58

Note that a load disturbance is applied to the motor to testify the robustness of the proposed control scheme. The experimental results shown in Fig. 12(b) reveal that the proposed control scheme is robust against the load disturbance.

In addition, the effects of model uncertainties on tracking performance are also studied, wherein values of the nominal parameters in controller model are uncertainty. According to (8), variations in parameters J_m and T_{fmap} are selected as representatives to testify the effectiveness of the proposed control scheme. The experimental results, as given in Table II, show that the proposed control scheme is effective for the considered model uncertainties.

VI. CONCLUSION

To compensate for cogging torque disturbance, a RONO was proposed to estimate the cogging torque for a PMDC torque motor, and an observer-based speed controller was designed through the triple-step nonlinear method. From the application point of view, the robustness analyses of observer and controller were discussed, respectively. Finally, the confirmatory tests were completed by using the AGV drives as follows.

1) The fundamental frequency of the torque harmonic was obtained through three different steady-state tracking experiments.
2) The observation results show that the designed observer has a fast enough convergence.
3) The compensation results show that the tracking errors at low speeds are substantially reduced by the proposed control scheme.
4) The comparative results show that the proposed control scheme has a better tracking performance than that of the other three control schemes.

ACKNOWLEDGMENT

The authors would like to thank Y. Wang and T. Qu for the BMI implementation, and also the Editors and all the anonymous reviewers for their valuable insights and comments.

REFERENCES

[1] R. Wang, C. Hu, F. Yan, and M. Chadli, "Composite nonlinear feedback control for path following of four-wheel independently actuated autonomous ground vehicles," *IEEE Trans. Intell. Transp. Syst.*, vol. 17, no. 7, pp. 2063–2074, Jul. 2016.

[2] N. Bianchi and S. Bolognani, "Design techniques for reducing the cogging torque in surface-mounted PM motors," *IEEE Trans. Ind. Appl.*, vol. 38, no. 5, pp. 1259–1265, Sep./Oct. 2002.

[3] W.-H. Chen, "Disturbance observer based control for nonlinear systems," *IEEE/ASME Trans. Mechatronics*, vol. 9, no. 4, pp. 706–710, Dec. 2004.

[4] S. Li, J. Yang, W.-H. Chen, and X. Chen, *Disturbance Observer-Based Control: Methods and Applications*. Boca Raton, FL, USA: CRC Press, 2014.

[5] M. Iwasaki, T. Shibata, and N. Matsui, "Disturbance-observer-based nonlinear friction compensation in table drive system," *IEEE/ASME Trans. Mechatronics*, vol. 4, no. 1, pp. 3–8, Mar. 1999.

[6] S. Li, J. Yang, W. H. Chen, and X. Chen, "Generalized extended state observer based control for systems with mismatched uncertainties," *IEEE Trans. Ind. Electron.*, vol. 59, no. 12, pp. 4792–4802, Dec. 2012.

[7] S. E. Talole, J. P. Kolhe, and S. B. Phadke, "Extended-state-observer-based control of flexible-joint system with experimental validation," *IEEE Trans. Ind. Electron.*, vol. 57, no. 4, pp. 1411–1419, Apr. 2010.

[8] D. G. Luenberger, "Observing the state of a linear system," *IEEE Trans. Mil. Electron.*, vol. 8, no. 2, pp. 74–80, Apr. 1964.

[9] L. Harnefors and M. Hinkkanen, "Complete stability of reduced-order and full-order observers for sensorless IM drives," *IEEE Trans. Ind. Electron.*, vol. 55, no. 3, pp. 1319–1329, Mar. 2008.
[10] W.-H. Chen, D. J. Ballance, P. J. Gawthrop, and J. O'Reilly, "A nonlinear disturbance observer for robotic manipulators," *IEEE Trans. Ind. Electron.*, vol. 47, no. 4, pp. 932–938, Aug. 2000.
[11] B. Gao, H. Chen, H. Zhao, and K. Sanada, "A reduced-order nonlinear clutch pressure observer for automatic transmission," *IEEE Trans. Control Syst. Technol.*, vol. 18, no. 2, pp. 446–453, Mar. 2010.
[12] N. Matsui, T. Makino, and H. Satoh, "Autocompensation of torque ripple of direct drive motor by torque observer," *IEEE Trans. Ind. Appl.*, vol. 29, no. 1, pp. 187–194, Jan. 1993.
[13] A. A. Godbole, J. P. Kolhe, and S. E. Talole, "Performance analysis of generalized extended state observer in tackling sinusoidal disturbances," *IEEE Trans. Control Syst. Technol.*, vol. 21, no. 6, pp. 2212–2223, Nov. 2013.
[14] W.-H. Chen, "Harmonic disturbance observer for nonlinear systems," *J. Dyn. Syst., Meas. Control*, vol. 125, no. 1, pp. 114–117, 2003.
[15] M. Ruderman, A. Ruderman, and T. Bertram, "Observer-based compensation of additive periodic torque disturbances in permanent magnet motors," *IEEE Trans. Ind. Informat.*, vol. 9, no. 2, pp. 1130–1138, May 2013.
[16] W. Wu, "A cogging torque compensating disturbance estimator for dc motor speed regulation: Design and experimentation," in *Proc. IEEE Int. Symp. Ind. Electron.*, Jul. 2009, pp. 368–372.
[17] H. Olsson, K. Åström, C. C. de Wit, M. Gäfvert, and P. Lischinsky, "Friction models and friction compensation," *Eur. J. Control*, vol. 4, no. 3, pp. 176–195, 1998.
[18] F. Al-Bender and J. Swevers, "Characterization of friction force dynamics," *IEEE Control Syst. Mag.*, vol. 28, no. 6, pp. 64–81, Dec. 2008.
[19] C. C. de Wit, H. Olsson, K. J. Astrom, and P. Lischinsky, "A new model for control of systems with friction," *IEEE Trans. Autom. Control*, vol. 40, no. 3, pp. 419–425, Mar. 1995.
[20] M. Ruderman, "Tracking control of motor drives using feedforward friction observer," *IEEE Trans. Ind. Electron.*, vol. 61, no. 7, pp. 3727–3735, Jul. 2014.
[21] Z. Jamaludin, H. V. Brussel, and J. Swevers, "Friction compensation of an XY feed table using friction-model-based feedforward and an inverse-model-based disturbance observer," *IEEE Trans. Ind. Electron.*, vol. 56, no. 10, pp. 3848–3853, Oct. 2009.
[22] J. Yao, W. Deng, and Z. Jiao, "Adaptive control of hydraulic actuators with LuGre model-based friction compensation," *IEEE Trans. Ind. Electron.*, vol. 62, no. 10, pp. 6469–6477, Oct. 2015.
[23] J. Yao, Z. Jiao, and D. Ma, "Rise-based precision motion control of DC motors with continuous friction compensation," *IEEE Trans. Ind. Electron.*, vol. 61, no. 12, pp. 7067–7075, Dec. 2014.
[24] B. Gao, H. Chen, Q. Liu, and H. Chu, "Position control of electric clutch actuator using a triple-step nonlinear method," *IEEE Trans. Ind. Electron.*, vol. 61, no. 12, pp. 6995–7003, Dec. 2014.
[25] K. R. S. Kodagoda, W. S. Wijesoma, and E. K. Teoh, "Fuzzy speed and steering control of an AGV," *IEEE Trans. Control Syst. Technol.*, vol. 10, no. 1, pp. 112–120, Jan. 2002.
[26] L. Harnefors, S. E. Saarakkala, and M. Hinkkanen, "Speed control of electrical drives using classical control methods," *IEEE Trans. Ind. Appl.*, vol. 49, no. 2, pp. 889–898, Mar./Apr. 2013.
[27] J. Han, "From PID to active disturbance rejection control," *IEEE Trans. Ind. Electron.*, vol. 56, no. 3, pp. 900–906, Mar. 2009.
[28] M. Iwasaki and N. Matusi, "Robust speed control of IM with torque feedforward control," *IEEE Trans. Ind. Electron.*, vol. 40, no. 6, pp. 553–560, Dec. 1993.
[29] A. Pisano, A. Davila, L. Fridman, and E. Usai, "Cascade control of PM DC drives via second-order sliding-mode technique," *IEEE Trans. Ind. Electron.*, vol. 55, no. 11, pp. 3846–3854, Nov. 2008.
[30] S. Z. Moussavi, M. Alasvandi, and S. Javadi, "PMDC motor speed control optimization by implementing ANFIS and MRAC," *Int. J. Control Sci. Eng.*, vol. 4, no. 1, pp. 1–8, 2014.
[31] J. Yao, Z. Jiao, and D. Ma, "Adaptive robust control of DC motors with extended state observer," *IEEE Trans. Ind. Electron.*, vol. 61, no. 7, pp. 3630–3637, Jul. 2014.
[32] H. Chen, X. Gong, Q. Liu, and Y. Hu, "Triple-step method to design nonlinear controller for rail pressure of gasoline direct injection engines," *IET Control Theory Appl.*, vol. 8, no. 11, pp. 948–959, Jul. 2014.
[33] B. Armstrong-Helouvry, *Control of Machines With Friction*, vol. 4. Berlin, Germany: Springer, 1991.
[34] T. Li and G. Slemon, "Reduction of cogging torque in permanent magnet motors," *IEEE Trans. Magn.*, vol. 24, no. 6, pp. 2901–2903, Nov. 1988.
[35] B. Rashidi, M. Esmaeilpour, and M. R. Homaeinezhad, "Precise angular speed control of permanent magnet DC motors in presence of high modeling uncertainties via sliding mode observer-based model reference adaptive algorithm," *Mechatronics*, vol. 28, pp. 79–95, Jun. 2015.
[36] J. G. VanAntwerp and R. D. Braatz, "A tutorial on linear and bilinear matrix inequalities," *J. Process Control*, vol. 10, no. 4, pp. 363–385, Aug. 2000.
[37] Q. T. Dinh, S. Gumussoy, W. Michiels, and M. Diehl, "Combining convex–concave decompositions and linearization approaches for solving BMIs, with application to static output feedback," *IEEE Trans. Autom. Control*, vol. 57, no. 6, pp. 1377–1390, Jun. 2012.
[38] M. Krstić, I. Kanellakopoulos, and P. Kokotović, *Nonlinear and Adaptive Control Design*. New York, NY, USA: Wiley-Interscience, 1995.
[39] M. Iwasaki, K. Seki, and Y. Maeda, "High-precision motion control techniques: A promising approach to improving motion performance," *IEEE Ind. Electron. Mag.*, vol. 6, no. 1, pp. 32–40, Mar. 2012.
[40] P. H. Chang and H. S. Park, "Time-varying input shaping technique applied to vibration reduction of an industrial robot," *Control Eng. Pract.*, vol. 13, no. 1, pp. 121–130, Jan. 2005.

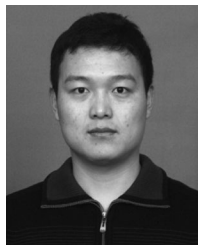

Hongqing Chu was born in Shandong, China. He received the B.S. degree in vehicle engineering from Shandong University of Technology, Zibo, China, in 2012. He is currently working toward the Ph.D. degree in control theory and control engineering at Jilin University, Changchun, China.

His current research interests include nonlinear control of dc motor drives, and vehicle powertrain control.

Bingzhao Gao was born in Shandong Province, China. He received the B.S. degree in vehicle engineering from Jilin University of Technology, Changchun, China, in 1998, the M.S. degree in vehicle engineering from Jilin University, Changchun, in 2002, and the Ph.D. degree in mechanical engineering from Yokohama National University, Yokohama, Japan, in 2009, and the Ph.D. degree in control engineering from Jilin University, Changchun, in 2009.

He is currently a Professor at Jilin University. His research interests include vehicle powertrain control and vehicle stability control.

Wanli Gu was born in Henan, China. He received the B.S. degree in electronic engineering from Jilin University, Changchun, China, in 2007, where he is currently working toward the Ph.D. degree in control theory and control engineering.

His current research interests include mobile robot control and dc motor control.

Hong Chen (M'02–SM'12) was born in Zhejiang, China. She received the B.S. and M.S. degrees in process control from Zhejiang University, Hangzhou, China, in 1983 and 1986, respectively, and the Ph.D. degree in system dynamics and control engineering from the University of Stuttgart, Stuttgart, Germany, in 1997.

Since 1999, she has been a Professor at Jilin University, Changchun, China, where she currently serves as Tang Aoqing Professor and as the Director of the State Key Laboratory of Automotive Simulation and Control. Her current research interests include model predictive control, optimal and robust control, nonlinear control, and applications in mechatronic systems focusing on automotive systems.